Supporting Information

Electrochemical Strategy for Hydrazine Synthesis: Development and Overpotential Analysis of Methods for Oxidative N–N Coupling of an Ammonia Surrogate

*Fei Wang, James B. Gerken, Desiree M. Bates, Yeon Jung Kim, Shannon S. Stahl**

Department of Chemistry, University of Wisconsin-Madison, 1101 University Avenue

Madison, WI, 53706, United States

stahl@chem.wisc.edu

Table of Contents:

1. General Experimental Considerations

1.1 Solvent and Reagents: organic solvents were obtained from an LC Technology Solutions Inc. solvent purification system using columns containing molecular sieves under argon; all commercially available compounds were used as received.

1.2 Characterization of Products: ^{1}H, ^{13}C, and ^{19}F NMR spectra were recorded on Bruker 400 or 500 MHz spectrometers. Chemical shifts are given in parts per million (ppm) relative to residual solvent peaks in the ^{1}H and ^{13}C NMR spectra or are referenced as noted. The following abbreviations (and their combinations) are used to label the multiplicities: s (singlet), d (doublet), t (triplet), m (multiplet) and br (broad). High-resolution mass spectra were obtained using a Thermo Q ExactiveTM Plus by the mass spectrometry facility at the University of Wisconsin. Chromatographic purification of products was accomplished by chromatography on silica gel 60 M (particle size 40-63 μm, 230-400 mesh) from MACHEREY-NAGEL Inc. Thin-layer chromatography (TLC) was performed on Silicycle silica gel UV254 pre-coated plates (0.25 mm).

1.3 Voltammetry Experiments: all cyclic voltammetric (CV) experiments were performed using Nuvant Array PGStats, from Nuvant System Inc. The experiments were carried out in a three-electrode cell configuration with a glassy carbon (GC) working electrode (3 mm diameter), and a platinum wire counter electrode (~ 1.0 cm, spiral wire). The working electrode potentials were measured versus $Ag/AgNO_3$ reference electrode (internal solution, 0.1 M Bu_4NClO_4 and 0.01 M $AgNO_3$ in CH_3CN). The redox potential of ferrocene/ferrocenium (Fc^+/Fc) was measured (same experimental conditions) and used to provide an internal reference. The potential values were then adjusted relative to Fc^+/Fc, and electrochemical studies in organic solvents were recorded accordingly. The GC working electrode was polished with alumina powder (5 μm) before each experiment.

2. General Procedures for Bulk Electrolysis (BE)

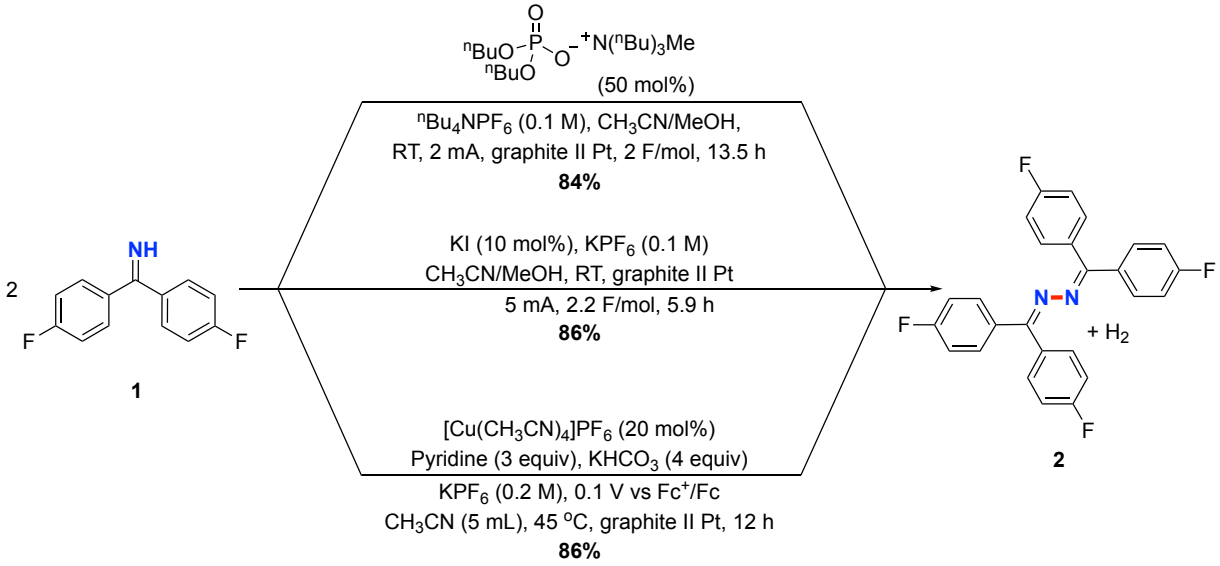

Scheme S1. Optimized conditions for bulk eletrolysis

2.1 Phosphate-promoted electrolysis (undivided cell): Reactions were carried out with a graphite rod anode (0.6 cm OD x 6 cm L, ~ 3 cm was immersed in the solution, apparent surface area ~ 6 cm^2), a platinum wire cathode (~1.0 cm, spiral wire) and a Ag^+/Ag reference electrode. A mixture of **1** (0.5 mmol, 1.0 equiv), nBu_4NPF_6 (0.5 mmol, 0.1 M) as supporting electrolyte, $[MeBu_3N][OP(O)(OBu)_2]$ (0.25 mmol, 50 mol%), and MeOH (4.0 mmol, 8.0 equiv) in acetonitrile (5 mL) was electrolyzed under constant current at 2 mA with magnetic stirring. The reaction was stopped automatically after passing 2 F/mol (13.5 h). The reaction was analyzed by crude ^{19}F NMR spectroscopy with α,α,α-trifluorotoluene as internal standard.

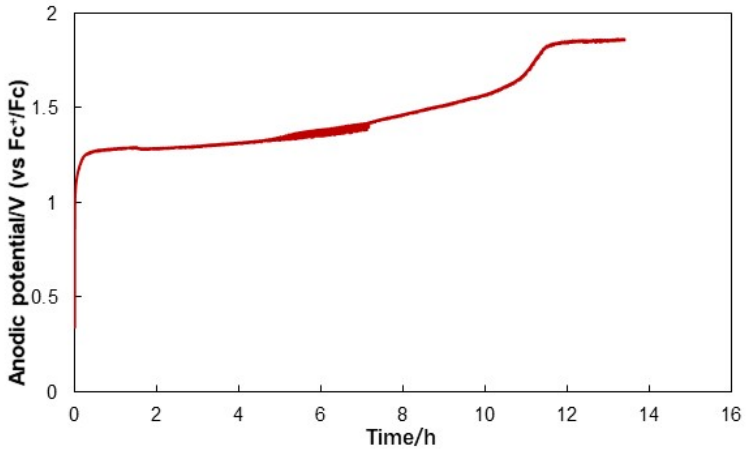

Figure S1. Representative anodic potential trace of phosphate-promoted electrolysis

2.2 Iodide-mediated electrolysis (undivided cell): Reactions were carried out with a graphite rod anode (0.6 cm OD x 6 cm L, ~ 3 cm was immersed in the solution, apparent surface area ~ 6 cm^2), a platinum wire cathode (~1.0 cm, spiral wire) and a Ag^+/Ag reference electrode. A mixture of **1** (0.5 mmol, 1.0 equiv), KPF_6 (0.5 mmol, 0.1 M), KI (0.05 mmol, 10 mol%), and MeOH (6.0 mmol, 12.0 equiv) in acetonitrile (5 mL) was electrolyzed under constant current at 5 mA with magnetic stirring. The reaction was stopped automatically after passing 2.2 F/mol (5.9 h). The reaction was analyzed by crude ^{19}F NMR spectroscopy with α,α,α-trifluorotoluene as internal standard.

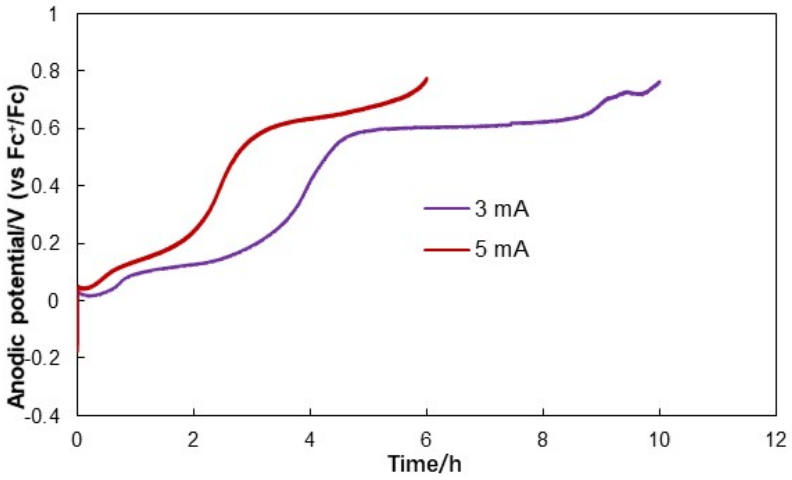

Figure S2. Representative anodic potential traces of iodide-mediated electrolysis

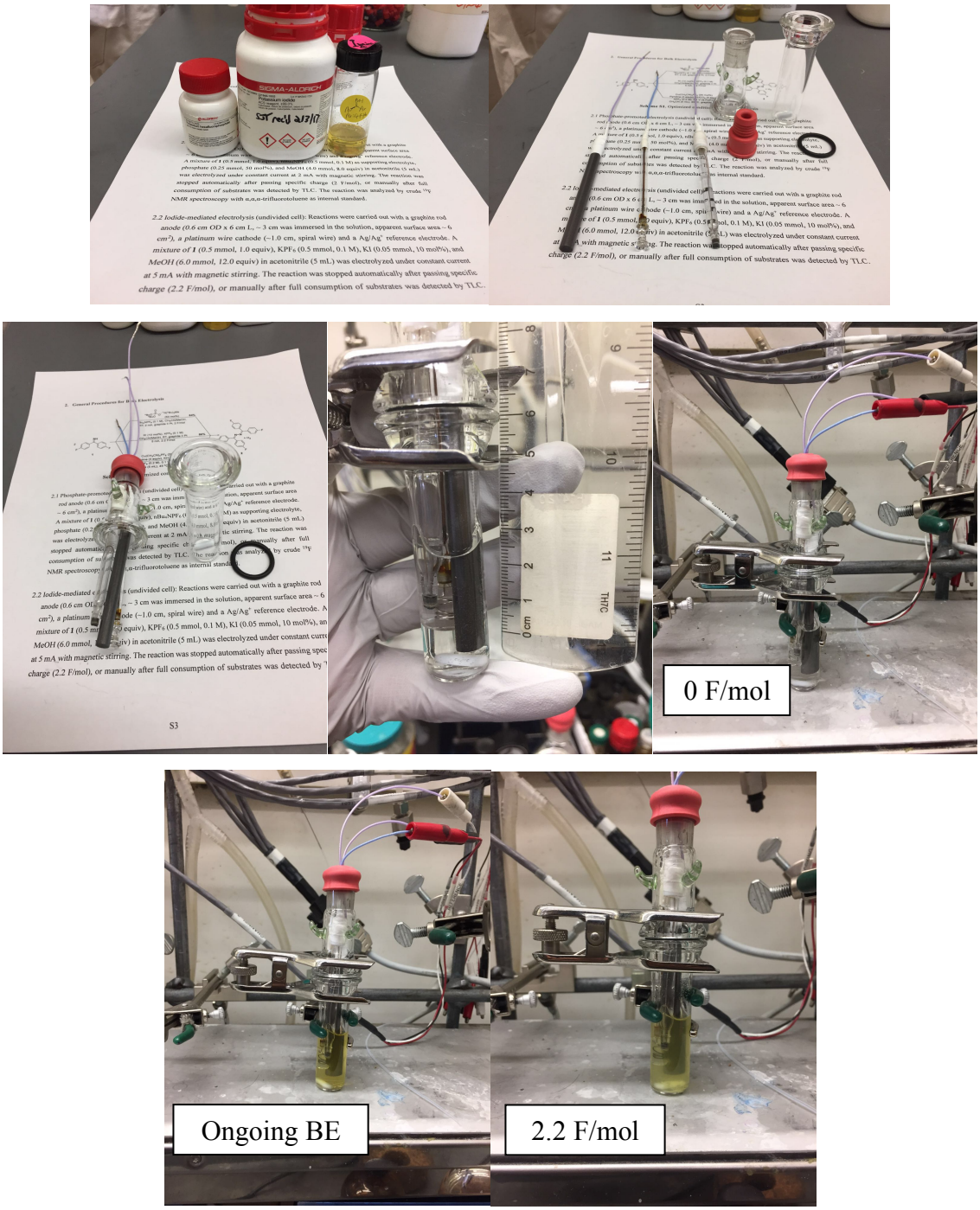

Figure S3. Graphical guide for iodide-mediated electrochemical imine (**1**) homocoupling.

2.3 Copper-mediated electrolysis (divided cell): Reactions were carried out with a graphite rod anode (0.6 cm OD x 6 cm L, ~ 4 cm was immersed in the solution, apparent surface area ~ 7.5 cm^2), a platinum wire cathode (~1.0 cm, spiral wire) and a Ag^+/Ag reference electrode. In the anodic chamber, **1** (0.5 mmol), $[Cu(CH_3CN)_4]PF_6$ (0.1 mmol, 20 mol%), pyridine (1.5 mmol, 3 equiv.), $KHCO_3$ (2.0 mmol, 4 equiv.), KPF_6 (1.0 mmol, 0.2 M) were added into CH_3CN (5.0 mL). In the cathodic chamber was placed KPF_6 (1.0 mmol, 0.2 M), MeOH (4 mmol, 0.8 M) and CH_3CN (5.0 mL). The solution was purged with nitrogen for 10 min, after which the bulk electrolysis was performed at 45 °C under constant potential at 0.1 V vs Fc^+/Fc. At the starting point, a yellow solution was observed that arised from coordination of imine with copper. The yellow color disappeared after charging for about 30 min. The initial current was around 6 mA (± 1 mA) and decreased to less than 1 mA after about 4 h. The reaction was allowed to run for 12 h and at that time the current reached to baseline. Then, solution in both chambers were collected and analyzed by crude ^{19}F NMR spectroscopy with α,α,α-trifluorotoluene as internal standard.

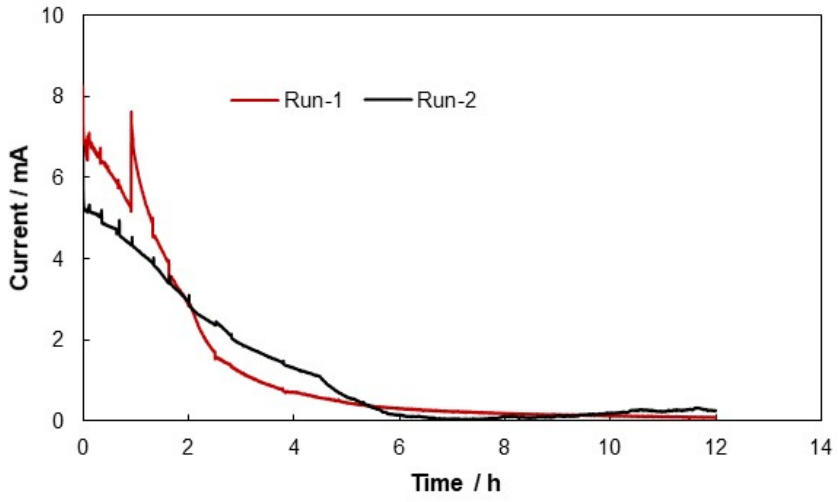

Figure S4. Representative current traces of Cu-mediated electrolysis under constant potential

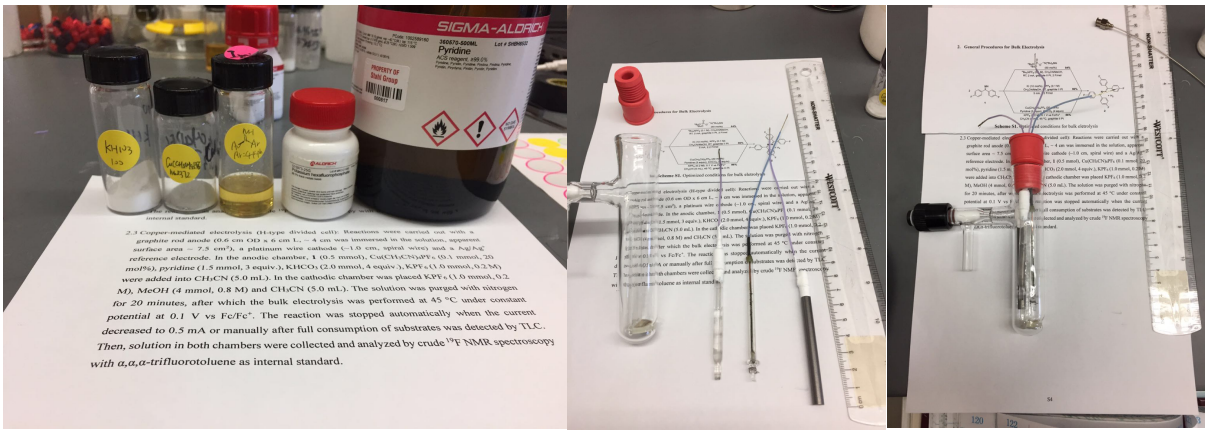

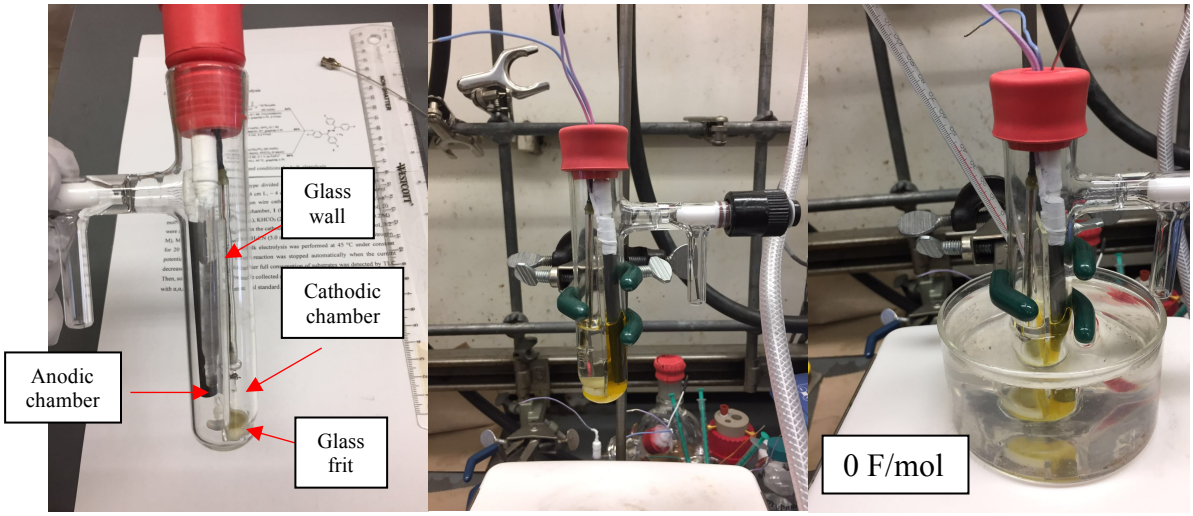

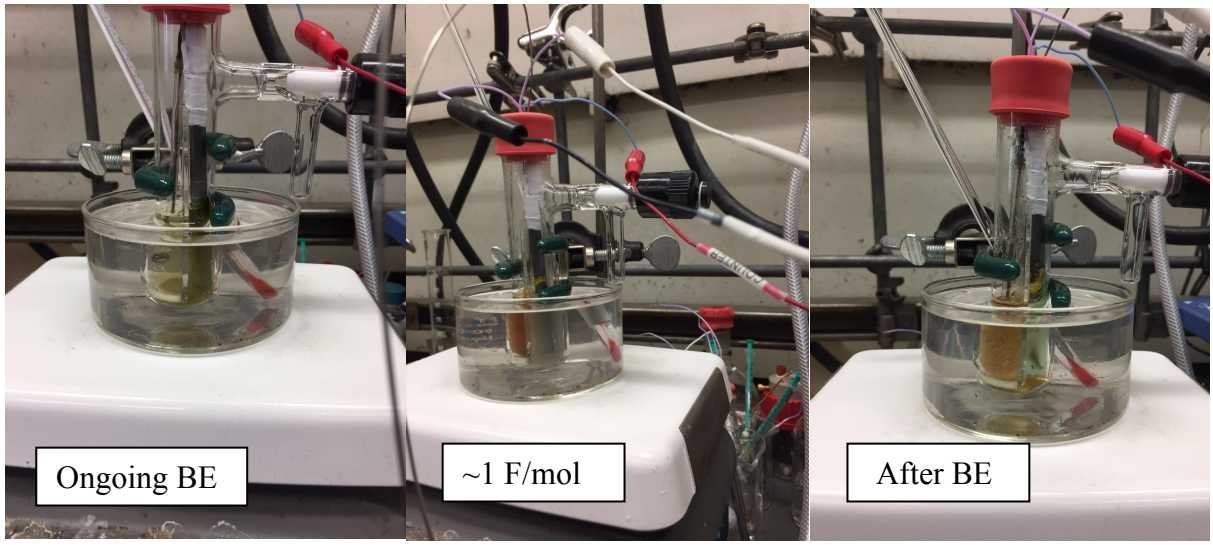

(continued on next page)

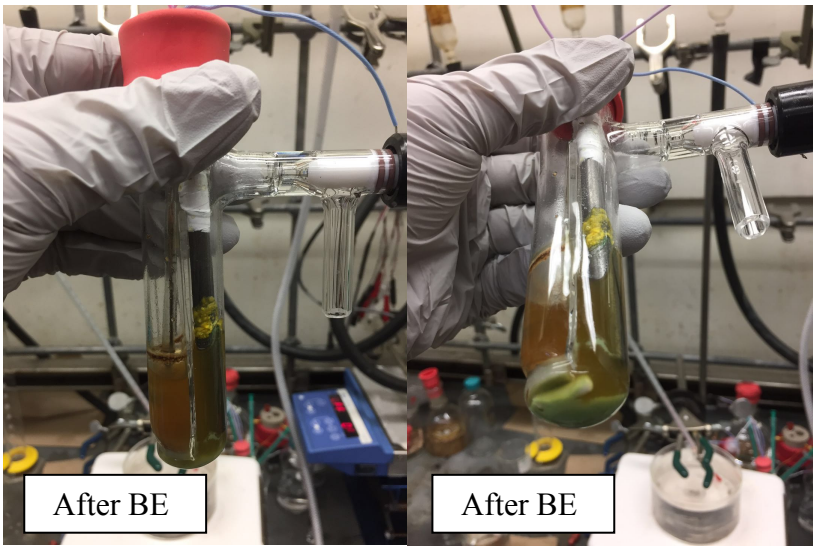

Figure S5. Graphical guide for Cu-mediated electrochemical imine (**1**) homocoupling.

3. Optimization of Reaction Conditions

Table S1. Base-promoted electrolysis

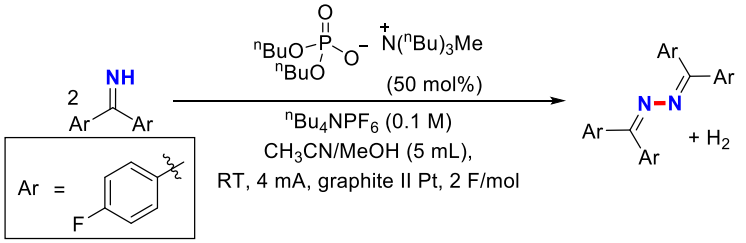

Entry	Base	Co-solvent	Current/mA	Yield/%[a]
1	-	MeOH (8 eq.)	4	< 3%
2	2,4,6-Collidine (0.5 eq.)	MeOH (8 eq.)	4	35%
3	2,6-Lutidine (0.5 eq.)	MeOH (8 eq.)	4	10%
4	NaOAc (0.5 eq.)	MeOH (8 eq.)	4	n.d.
5	MeO-$PhCO_2Na$ (0.5 eq.)	MeOH (8 eq.)	4	n.d.
6	$N(^nBu)_3MeOP(O)(OBu)_2$ (0.5 eq.)	MeOH (8 eq.)	4	71%
7	$N(^nBu)_3MeOP(O)(OBu)_2$ (0.3 eq.)	MeOH (8 eq.)	4	65%
8	$N(^nBu)_3MeOP(O)(OBu)_2$ (0.1 eq.)	MeOH (8 eq.)	4	22%
9[b]	$N(^nBu)_3MeOP(O)(OBu)_2$ (1.0 eq.)	MeOH (8 eq.)	4	68%
10	$N(^nBu)_3MeOP(O)(OBu)_2$ (0.5 eq.)	CF_3CH_2OH (8 eq.)	4	25%
11	$N(^nBu)_3MeOP(O)(OBu)_2$ (0.5 eq.)	CF_3CH_2OH (12 eq.)	4	23%
12	$N(^nBu)_3MeOP(O)(OBu)_2$ (0.5 eq.)	-	4	35%
13	$N(^nBu)_3MeOP(O)(OBu)_2$ (0.5 eq.)	MeOH (8 eq.)	2	84%
14	$N(^nBu)_3MeOP(O)(OBu)_2$ (0.5 eq.)	MeOH (8 eq.)	6	33%
15	$N(^nBu)_3MeOP(O)(OBu)_2$ (0.5 eq.)	MeOH (8 eq.)	10	26%
16	$N(^nBu)_3MeOP(O)(OBu)_2$ (0.5 eq.)	MeOH (4 eq.)	2	84%
17	$N(^nBu)_3MeOP(O)(OBu)_2$ (0.5 eq.)	MeOH (12 eq.)	2	84%
18[c]	$N(^nBu)_3MeOP(O)(OBu)_2$ (0.5 eq.)	MeOH (8 eq.)	2	< 3%

[a]0.5 mmol scale with α,α,α-trifluorotoluene as internal standard. [b]Without $^nBu_4NPF_6$. [c]With reticulated vitreous carbon (RVC, 30 PPI, 0.635*1*2 cm^3, ~ 24 cm^2) as working electrode.

Reactions were conducted following the general procedure shown in section 2.1, and deviations from the optimized conditions and corresponding yields were listed in Table **S1**.

Table S2. Iodide-mediated electrolysis

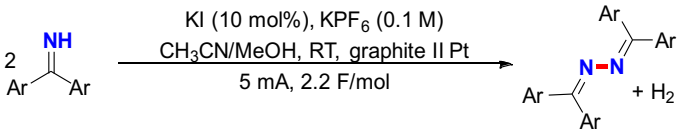

Entry	Catalysis	Co-solvent	Current/mA	Charge	Yield/%[a]
1	$^{n}Bu_4NI$ (5 mol%)	-	5	3 F/mol	< 3%
2	$^{n}Bu_4NI$ (5 mol%)	MeOH (8 eq.)	5	3 F/mol	38%
3	$^{n}Bu_4NI$ (5 mol%)	CF_3CH_2OH (8 eq.)	5	3 F/mol	33%
4	$^{n}Bu_4NI$ (5 mol%)	HFIP (8 eq.)	5	3 F/mol	19%
5	KI (5 mol%)	MeOH (8 eq.)	5	3 F/mol	61%
6	Et_4NBr (5 mol%)	MeOH (8 eq.)	5	3 F/mol	n.d.
7	$^{n}Bu_4NCl$ (5 mol%)	MeOH (8 eq.)	5	3 F/mol	n.d.
8	KI (5 mol%)	MeOH (8 eq.)	5	2.2 F/mol	74%
9	KI (5 mol%)	MeOH (4 eq.)	5	2.2 F/mol	67%
10	KI (5 mol%)	MeOH (12 eq.)	5	2.2 F/mol	82%
11	KI (7.5 mol%)	MeOH (8 eq.)	5	2.2 F/mol	80%
12	KI (10 mol%)	MeOH (8 eq.)	5	2.2 F/mol	84%
13	KI (10 mol%)	MeOH (12 eq.)	5	2.2 F/mol	86%
14	KI (10 mol%)	MeOH (12 eq.)	5	2.0 F/mol	81%
15	KI (10 mol%)	MeOH (12 eq.)	5	1.8 F/mol	75%
16	KI (10 mol%)	MeOH (12 eq.)	5	1.5 F/mol	38%
17	KI (10 mol%)	MeOH (12 eq.)	5	1.2 F/mol	8%
18	KI (10 mol%)	MeOH (12 eq.)	3	2.2 F/mol	84%
19	KI (10 mol%)	MeOH (12 eq.)	8	2.2 F/mol	86%

[a]0.5 mmol scale with α,α,α-trifluorotoluene as internal standard. n.d. = not detected.

Reactions were conducted following the general procedure shown in section 2.2, and deviations from the optimized conditions and corresponding yields were listed in Table **S2**.

Table S3. Copper-mediated electrolysis

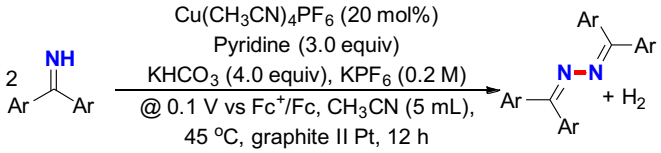

Entry	Deviation from standard conditions	Yield/%[a]
1	none	86
2	K_2CO_3 instead of $KHCO_3$	34
3	K_3PO_4 instead of $KHCO_3$	4
4	$NaHCO_3$ instead of $KHCO_3$	54
5	without $KHCO_3$	15
6	$TBAPF_6$ instead of KPF_6	79
7	2 equiv of pyridine	75
8	4 equiv of pyridine	86
9	at room temperature	46
10	applied potential @ 0 mV vs Fc/Fc^+	72
11	10 mol% Cu(I)	77

[a]0.5 mmol scale with α,α,α-Trifluorotoluene as internal standard.

Reactions were conducted following the general procedure shown in section 2.3, and deviations from the optimized conditions and corresponding yields were listed in Table **S3**.

4. Cyclic Voltammetry Studies

The following CVs provide additional data beyond those shown in Figures 2B, 3B, and 4B in the manuscript.

4.1 Imine **1** with or without phosphate.

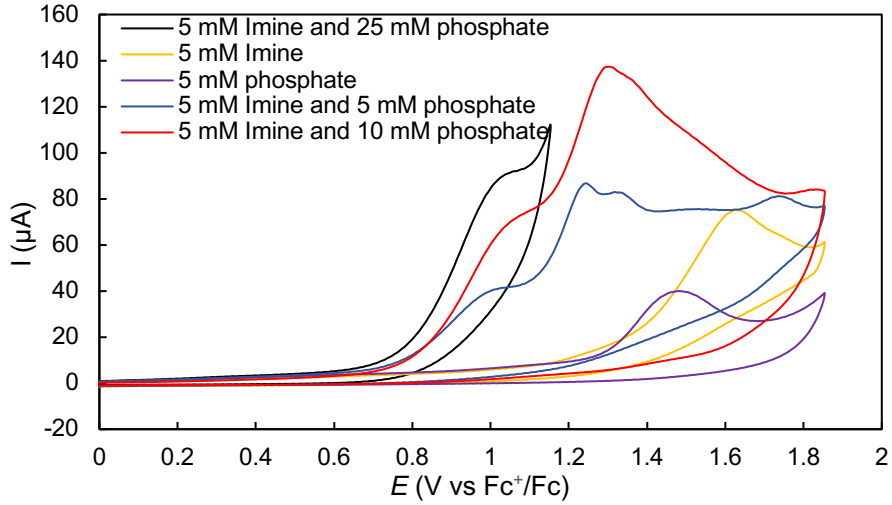

Figure S6. CV studies of **1** (5 mM) with or without phosphate in acetonitrile with $^{n}Bu_4NPF_6$ (0.1 M) as supporting electrolyte, glassy carbon as working electrode (~ 7.0 mm^2) and a platinum wire (1.0 cm, spiral wire) as counter electrode, scan rate = 20 mV/s.

4.2 Iodide-mediated conditions.

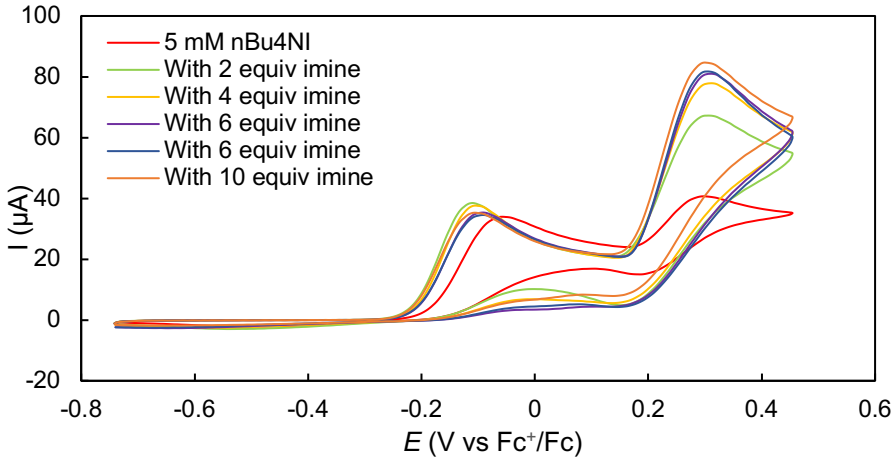

Figure S7. CV studies of $^{n}Bu_4NI$ with or without **1**. Conditions: 5 mM $^{n}Bu_4NI$ in CH_3CN (10 mL), 0.1 M $^{n}Bu_4NPF_6$ with different amount of **1**, glassy carbon as working electrode (~ 7.0 mm^2) and a platinum wire (1.0 cm, spiral wire) as counter electrode, scan rate = 20 mV/s.

4.3 CVs of Cu(I) with or without pyridine.

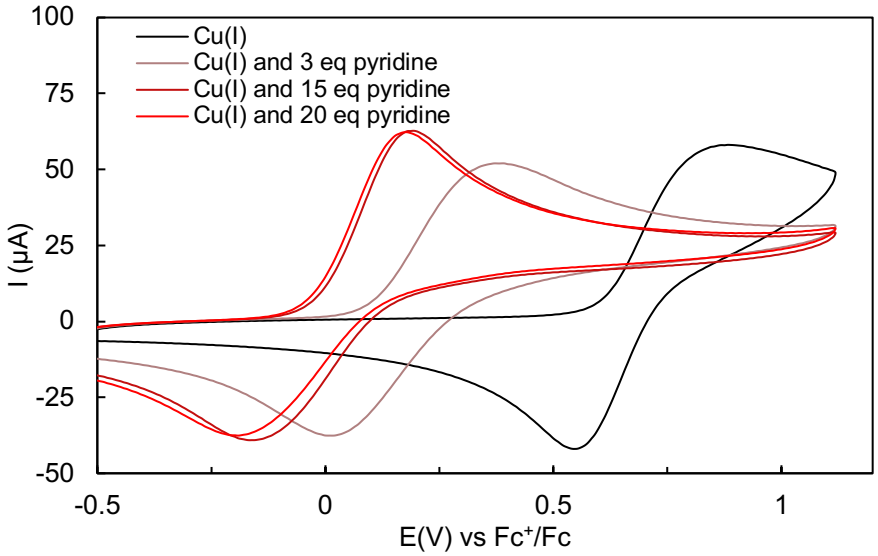

Figure S8. CV of $[Cu(CH_3CN)_4]PF_6$ (5 mM) and pyridine in acetonitrile with KPF_6 (0.1 M) as supporting electrolyte, glassy carbon as working electrode (~ 7.0 mm^2) and a platinum wire (1.0 cm, spiral wire) as counter electrode, scan rate = 100 mV/s.

4.4 CVs of Cu(I) in the presence of different concentration of imine **1**.

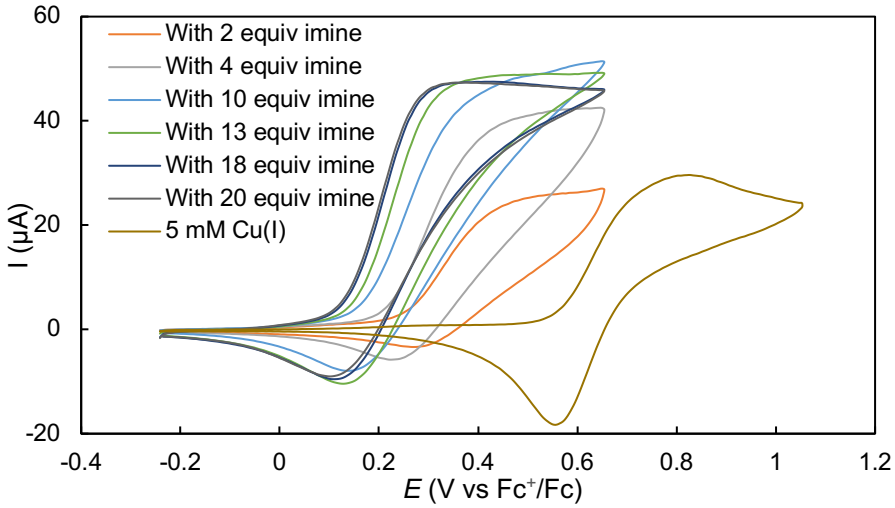

Figure S9. CV of $[Cu(CH_3CN)_4]PF_6$ (5 mM) and **1** in acetonitrile with $^nBu_4NPF_6$ (0.1 M) as supporting electrolyte, glassy carbon as working electrode (~ 7.0 mm^2) and a platinum wire (1.0 cm, spiral wire) as counter electrode, scan rate = 20 mV/s.

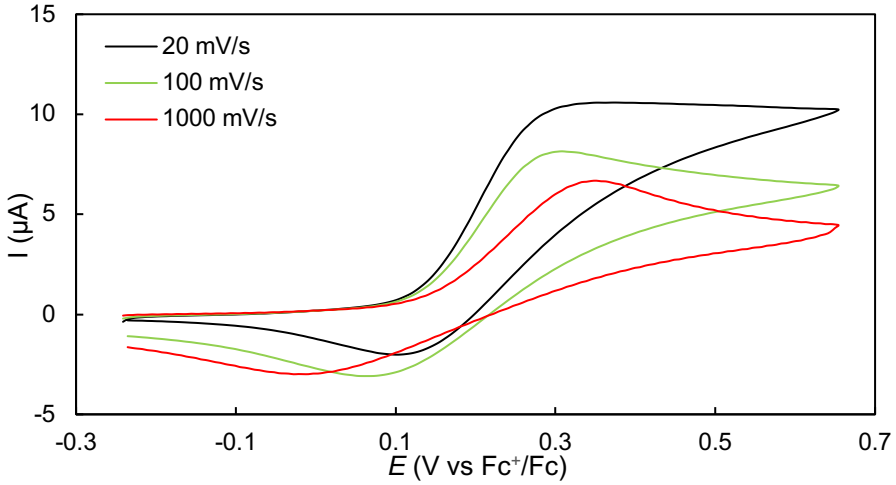

Figure S10. Normalized CV of $[Cu(CH_3CN)_4]PF_6$ (5 mM) and **1** (100 mM) at different scan rates in acetonitrile with $^nBu_4NPF_6$ (0.1 M) as supporting electrolyte, glassy carbon as working electrode (~ 7.0 mm^2) and a platinum wire (1.0 cm, spiral wire) as counter electrode.

The data in Figure S10 were modeled using the software ESP v. 2.4.[1] Using an oversimplified model, some kinetic parameters were able to be estimated. The model consisted of a reversible electrochemical step followed by a chemical step that is second-order in Cu^{+2} and that regenerates Cu^{+1}. It is expected that imine substrate will be coordinated to redox-active Cu species involved in these steps (i.e., L = imine or acetonitrile solvent). Using these assumptions, a fit of the experimental data led to a chemical rate constant for N–N coupling of 16 $M^{-1}s^{-1}$ (cf. second step in Figure S11). Although this value is only a rough estimation, it suggests that the bulk electrolysis experiments are limited by mass transport, rather than chemical kinetics, because the rate constant implies a reaction time of < 1 min, if it were limited solely by chemical kinetics.

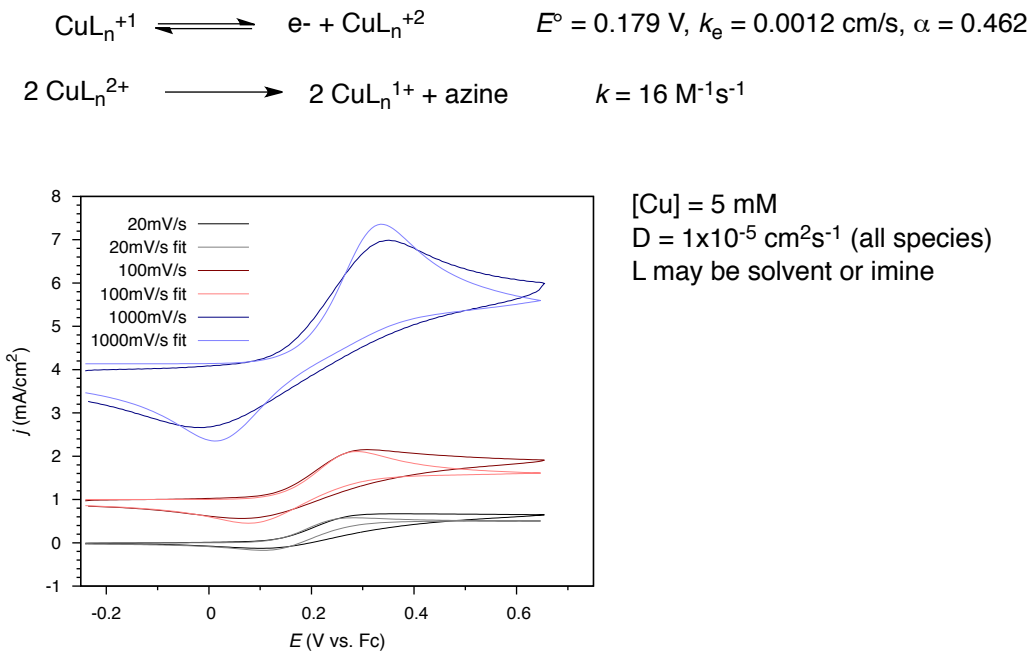

Figure S11. E-C model and parameters with simulated and experimental CV data at different scan rates, other conditions being equal. Experimental data are identical to those in Figure S10.

5. Pourbaix Diagram Data Collection and Thermodynamic Calculations

The experiments were carried out in a three-electrode cell configuration with a glassy carbon (GC) working electrode (3 mm diameter), and a platinum wire counter electrode (~1.0 cm, spiral wire), and $^{n}Bu_4NPF_6$ (0.1 M) as supporting electrolyte. The working electrode potentials were measured versus $Ag/AgNO_3$ reference electrode (internal solution, 0.1 M Bu_4NClO_4 and 0.01 M $AgNO_3$ in CH_3CN). The redox potential of ferrocene/ferrocenium (Fc^+/Fc) was measured (same experimental conditions) and the potential values were then adjusted relative to Fc^+/Fc. Because some of the peak currents were ill-defined, the inflection point of each relevant oxidation feature (the dots in Figures S12-S14) was chosen as an approximate $E_{1/2}$ for the Pourbaix analysis. The data of each entry was collected three times and reported as an average in the Pourbaix diagram. All of the experiments were conducted at room temperature.

Table S4. Different buffer conditions for acquistion of CV data used in the Pourbaix diagram

Entry	Mediator	Imine	2,6-Lutidine	2,4,6-Collidine	dibutyl phosphate	TfOH[b]	Scan rate
1	No	10 mM	No	No	No	5 mM	20 mV/s
2	No	5 mM	No	100 mM	No	50 mM	20 mV/s
3	No	5 mM	No	No	20 mM	10 mM	20 mV/s
4	$^{n}Bu_4NI$/5 mM	100 mM	No	No	No	50 mM	20 mV/s
5	$^{n}Bu_4NI$/5 mM	50 mM	100 mM	No	No	50 mM	20 mV/s
6	$^{n}Bu_4NI$/5 mM	50 mM	No	100 mM	No	50 mM	20 mV/s
7	$^{n}Bu_4NI$/5 mM	50 mM	No	No	100 mM	50 mM	20 mV/s
8[a]	Cu(I)/5 mM	200 mM	No	No	No	100 mM	20 mV/s
9[a]	Cu(I)/5 mM	100 mM	20 mM	No	No	10 mM	20 mV/s
10[a]	Cu(I)/5 mM	100 mM	No	20 mM	No	10 mM	20 mV/s

[a]Cu(I) refers to $[Cu(CH_3CN)_4]PF_6$; [b]TfOH refers to triflic acid.

Table S5. Redox potentials for imine oxidation and associated pK_as for the Pourbaix diagram

Entry	Mediator	Buffer p*K*a	Potential/V (vs Fc^+/Fc)[a]
1	No	13.3	1.45
2	No	14.98	1.30
3	No	18.2	1.2

4	$^{n}Bu_4NI$	13.3	0.28
5	$^{n}Bu_4NI$	14.13	0.25
6	$^{n}Bu_4NI$	14.98	0.26
7	$^{n}Bu_4NI$	18.2	0.30
8	$[Cu(CH_3CN)_4]PF_6$	13.3	0.20
9	$[Cu(CH_3CN)_4]PF_6$	14.13	0.23
10	$[Cu(CH_3CN)_4]PF_6$	14.98	0.23

[a]The potential refers to the inflection point of each related oxidation feature.

In a process similar to the one used to generate Scheme 1, literature data for the N_2/NH_4^+ and $N_2/N_2H_5^+$ potentials can be combined to produce the $N_2H_5^+/NH_4^+$ potential (Scheme S2).[2] With some further arithmetic utilizing Scheme 1C as well, the $N_2H_5^+/NH_3$ potential is obtained to cover the pK_a 16.5 to 16.6 region of the Pourbaix diagram in between the NH_4^+ and $N_2H_5^+$ pK_as. With the computed azine ammonolysis value and the experimentally measured iminium pK_a (vide infra), the potential for azine reduction to the iminium is obtained.

Scheme S2. Thermodynamic Data for Interconversion of $N_2/N_2H_5^+/NH_4^+$ and Azine/Iminium in MeCN

A) $N_2 + 8\,BH^+ + 6\,e^- \rightleftharpoons 2\,NH_4^+ + 8\,B$ — $\Delta G° = -49.9 + (8*1.364*pK_a)$ kcal/mol; $E° = 0.361 - (0.079*pK_a)$ V

B) $N_2 + 5\,BH^+ + 4\,e^- \rightleftharpoons N_2H_5^+ + 5\,B$ — $\Delta G° = 14.09 + (5*1.364*pK_a)$ kcal/mol; $E° = -0.153 - (0.074*pK_a)$ V

C) $N_2H_5^+ + 3\,BH^+ + 2\,e^- \rightleftharpoons 2\,NH_4^+ + 3\,B$ — $\Delta G° = -64.0 + (3*1.364*pK_a)$ kcal/mol; $E° = 1.388 - (0.085*pK_a)$ V

D) $N_2H_5^+ + 1\,BH^+ + 2\,e^- \rightleftharpoons 2\,NH_3 + 1\,B$ — $\Delta G° = -19.0 + (1*1.364*pK_a)$ kcal/mol; $E° = 0.412 - (0.029*pK_a)$ V

E) Imine (**1**) + 1 BH^+ $\rightleftharpoons$ Iminium + 1 B — $\Delta G° = -18.1 + (1*1.364*pK_a)$ kcal/mol

F) Azine (**2**) + 2 NH_3 $\rightleftharpoons$ 2 Imine (**1**) + N_2H_4 — $\Delta G° = 14.4$ kcal/mol

G) Azine (**2**) + 4 BH^+ + 2 e^- $\rightleftharpoons$ 2 Iminium + 4 B — $\Delta G° = -63.4 + (4*1.364*pK_a)$ kcal/mol; $E° = 1.375 - (0.118*pK_a)$ V

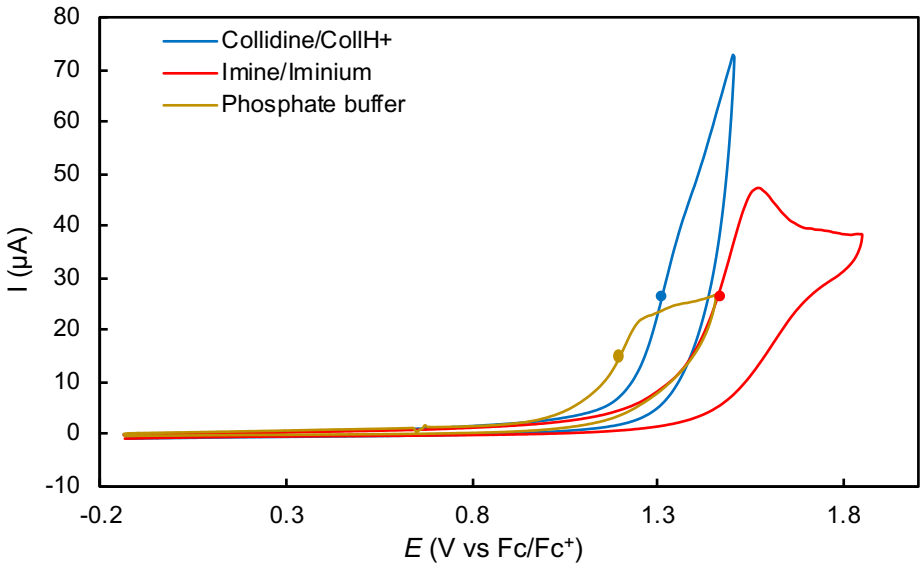

Figure S12. CVs of base-promoted system under different buffer conditions

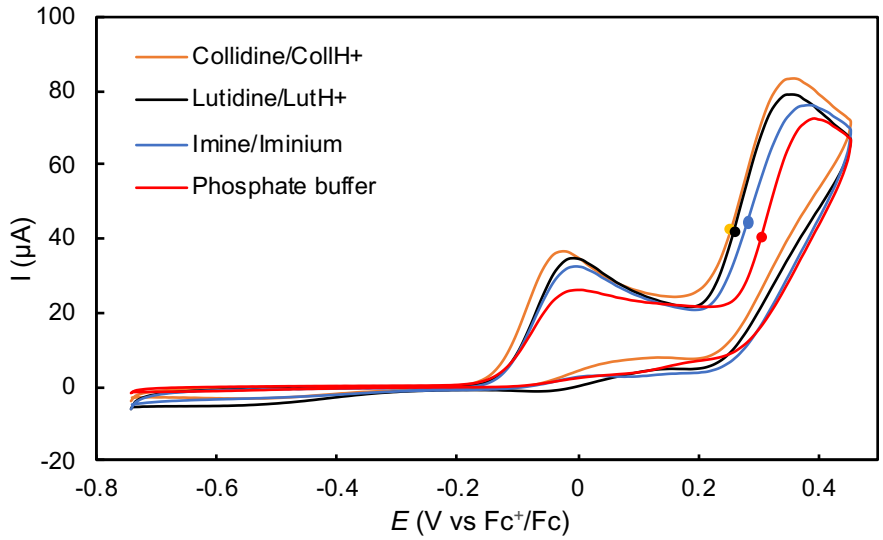

Figure S13. CVs of iodide-mediated system under different buffer conditions

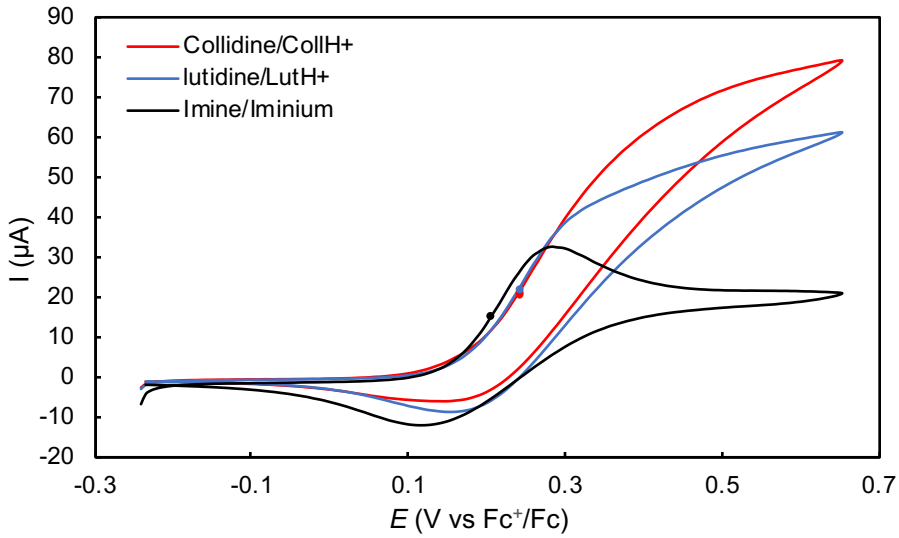

Figure S14. CVs of copper-mediated system under different buffer conditions

6. Iminium and Dibutylphosphate pK_a Determination.

NMR techniques were used to measure the pK_a values.[3] For the iminium pK_a, NMR spectra were taken of the imines in CD_3CN and in the presence of an excess of a relatively strong acid compared to the iminium (4-nitrobenzenesulfonic acid was used). Next, spectra of the imine in the presence of a test acid were taken. Reference spectra of each test acid and its conjugate base were also taken. Then, chemical shifts were put into eq S1, where δ_O is the observed δ of the imine in the presence of the test acid, δ_{HA} is the δ of the iminium, δ_A is the δ of the imine, δ_T is the observed δ of the test acid in the presence of the imine, δ_B is the δ of the test acid conjugate base, and δ_{HB} is the δ of the test acid. This procedure was repeated with various test acids until acids with closely spaced pK_as bracketing the calculated iminium pK_a gave a consistent result. From the ratio of K_{HA}/K_{HB}, the pK_a of the iminium (tabulated in the main text) is readily obtained by eq S2. The dibutylphosphate pK_a was measured similarly, using tosylic acid to obtain the fully-protonated form. To minimize ion-pairing effects, cationic acids were used to measure the iminium pK_a and neutral acids were used for the dibutylphosphate pK_a.

$$((\delta_O - \delta_{HA})/(\delta_A - \delta_O))*((\delta_T - \delta_B)/(\delta_{HB} - \delta_T)) = K_{HA}/K_{HB} \quad \text{(S1)}$$

$$pK_{a(HA)} = pK_{a(HB)} - \log_{10}(K_{HA}/K_{HB}) \quad \text{(S2)}$$

Table S6. Test acid and iminium pK_a values in acetonitrile

Test Acid	pK_a
2-methoxypyridinium	9.93[a]
N,N-dimethylanilinium	11.43[a]
pyridinium	12.53[a]
2,6-lutidinium	14.13[a]
2,4,6-collidinium	14.98[a]
2-aminobenzimidazolium	16.08[a]
4,4'-difluorobenzophenone iminium (**1**)	13.28
phthalic acid	14.3[b]
saccharin	14.57[b]
2-nitrobenzoic acid	18.2[b]
4-nitrobenzoic acid	18.7[b]
dibutylphosphonic acid	18.2

[a]The test acid pK_a values are from Ref. [4] [b]These test acid pK_a values are from Ref. [5]

7. Electrolysis under Buffered Conditions

7.1 Iodide-mediated electrolysis

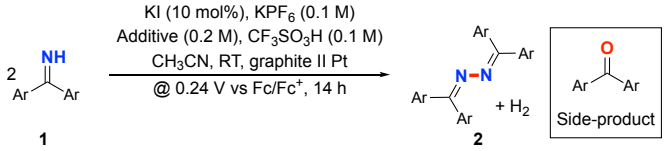

Entry	**1**/[M]	Additive	Side-product	Conversion	Yield
1	0.2	-	69%	71%	n.d.
2	0.1	2,4,6-Collidine	49%	57%	7%

Scheme S3. Iodide-mediated electrolysis under buffer conditions

Entry 1 (imine/iminium buffer): Reaction was carried out with a graphite anode (0.6 cm OD x 6 cm L, ~ 3 cm was immersed in the solution), a platinum wire cathode (1.0 cm, spiral wire) and a Ag^+/Ag reference electrode. A mixture of **1** (1 mmol), KPF_6 (0.5 mmol, 0.1 M) as supporting electrolyte, KI (0.05 mmol, 10 mol%), and triflic acid (0.5 mmol) in acetonitrile (5 mL) was electrolyzed overnight under constant potential at 0.24 V vs Fc^+/Fc with magnetic stirring. The result was analyzed by crude ^{19}F NMR spectroscopy with KPF_6 (supporting electrolyte) as internal standard, which showed that the substrate underwent hydrolysis predominatly with no N–N bond formation product.

Entry 2 (collidine/collidinium buffer): Reaction was carried out with a graphite anode (0.6 cm OD x 6 cm L, ~ 3 cm was immersed in the solution), a platinum wire cathode (1.0 cm, spiral wire) and a Ag^+/Ag reference electrode. A mixture of **1** (0.5 mmol), KPF_6 (0.5 mmol, 0.1 M) as supporting electrolyte, KI (0.05 mmol, 10 mol%), triflic acid (0.5 mmol) and 2,4,6-collidine (1.0 mmol) in acetonitrile (5 mL) was electrolyzed overnight under constant potential at 0.24 V vs Fc^+/Fc with magnetic stirring. The result was analyzed by crude ^{19}F NMR spectroscopy with KPF_6 (supporting electrolyte) as internal standard, which revealed that desired product was produced in a yield of 7%.

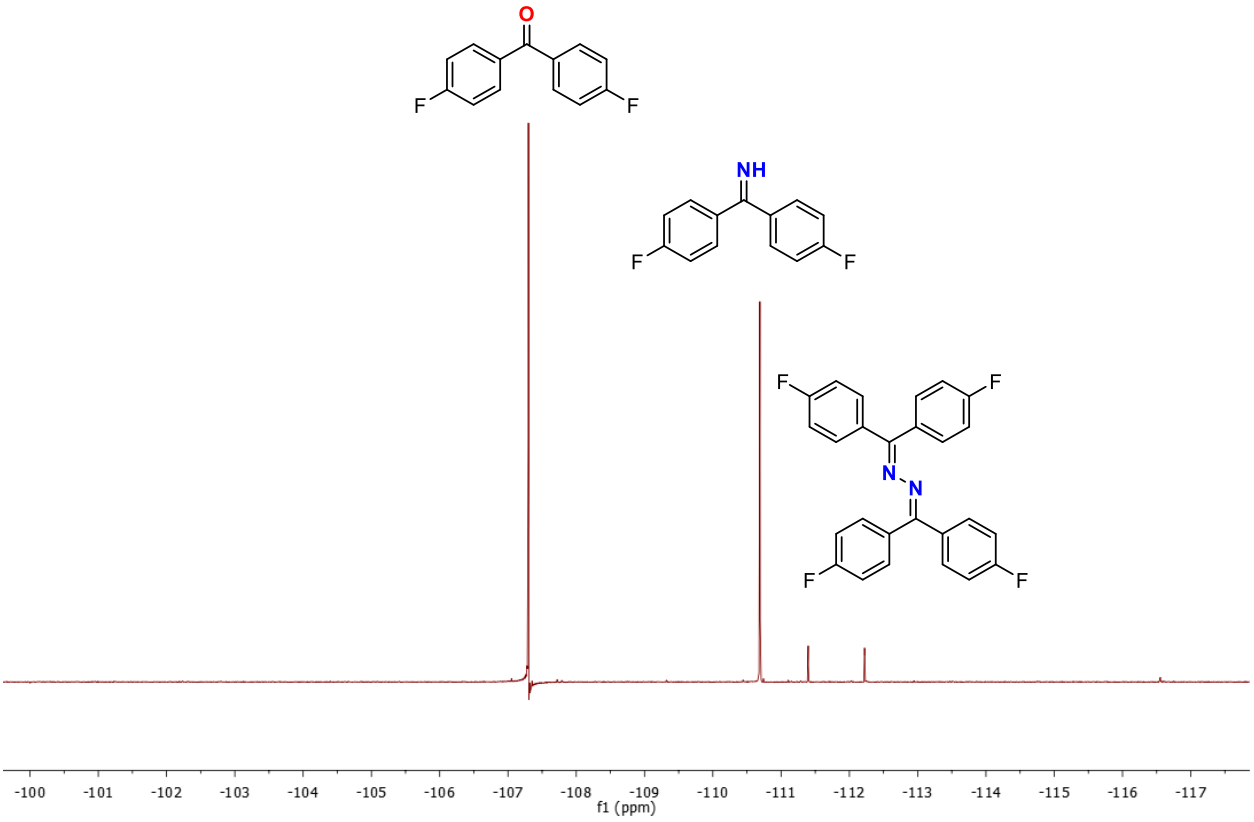

Figure S15. Crude ^{19}F NMR spectroscopy under collidine/collidinium buffer conditions

7.2 Copper-mediated electrolysis

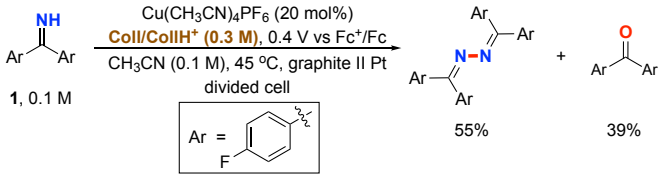

Scheme S4. Copper-mediated electrolysis under buffer conditions

Collidine/collidinium buffer: Reactions were carried out with a graphite rod anode (0.6 cm OD x 6 cm L, ~ 4 cm was immersed in the solution), a platinum wire cathode (1.0 cm, spiral wire) and a Ag/Ag^+ reference electrode. In the anodic chamber, **1** (0.5 mmol), $Cu(CH_3CN)_4PF_6$ (0.1 mmol, 20 mol%), 2,4,6-collidine (3.0 mmol, 6 equiv.) and triflic acid (1.5 mmol, 3 equiv.) were added into CH_3CN (5.0 mL). In the cathodic chamber was placed 2,4,6-collidine (1.5 mmol, 0.3 M),

triflic acid (1.5 mmol, 0.3 M) and CH_3CN (5.0 mL). The solution was purged with nitrogen for 10 min, after which the bulk electrolysis was performed under constant potential at 0.4 V vs Fc^+/Fc under 45 °C. The reaction was allowed to run overnight (14 h). After that, the solution in both chambers were collected and analyzed by crude ^{19}F NMR spectroscopy with Fluorobenzene as internal standard.

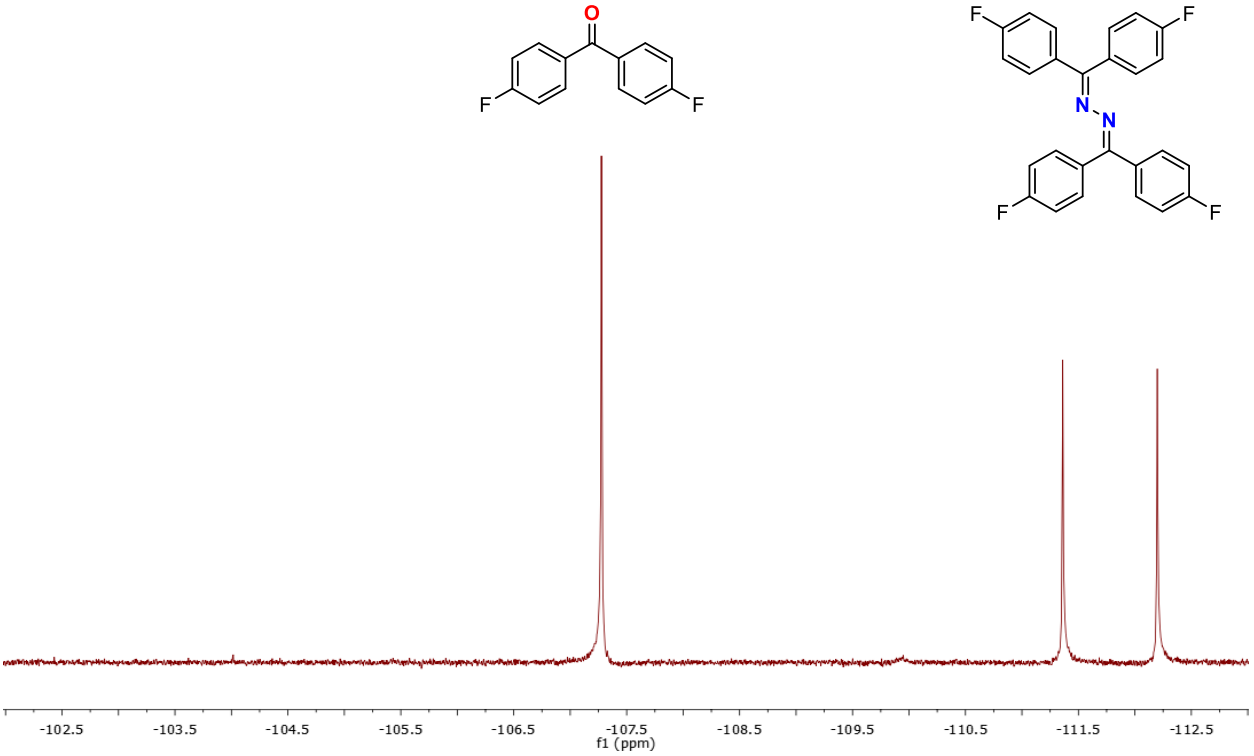

Figure S16. Crude ^{19}F NMR spectroscopy under collidine/collidinium buffer conditions

8. DFT calculations

All calculations employed density functional theory (DFT) using B3LYP functional in conjunction with 6-311+G(2d,p) basis set. Vibrational frequency calculations were performed to determine all structures are a minima on the potential energy surface and to determine the Gibbs Free energies at 298.15 K. All calculations used the Polarizable Continuum Model (PCM) to model a solvent. The solvent used is Acetonitrile. All calculations were performed using Gaussian 16.[6] All optimized structures, electronic and Gibbs free energies are reported below.

Table S7. DFT-Computed Energies.

Molecule	Electronic Energy (Hartrees)	Gibbs Free Energy (Hartrees)
NH_3	-56.5892746483	-56.573158
N_2H_4	-111.920594365	-111.88929
$C_{13}H_9F_2N$ (**1**)	-755.460027818	-755.314231
$C_{26}H_{16}F_4N_2$ (**2**)	-1509.68510168	-1509.394308

NH_3

N	-0.005034	0.00790441	-0.0037053
H	0.00249263	-0.0039142	1.01259596
H	0.9675813	-0.0039139	-0.2985686
H	-0.4056339	-0.8784588	-0.2985689

N_2H_4

N	0.000000	0.000000	0.000000
N	0.000000	-1.443396	0.000000
H	-0.951808	-1.742782	-0.182912
H	0.253397	-1.809660	0.915374
H	0.951808	0.299386	-0.182912
H	-0.253397	0.366264	0.915374

$C_{13}H_9F_2N$

C	2.68994467	-1.1555816	0.89990479
C	3.71119473	-0.7011175	0.08499314
C	3.56136382	0.37905347	-0.7662554
C	2.33666803	1.03430926	-0.7887588
C	1.27562478	0.60726342	0.01734229
C	1.46561314	-0.5003753	0.85091042
H	0.65772392	-0.8469647	1.48254143

C	-0.0122024	1.36597022	0.02434032
C	-1.2940249	0.60642984	-0.0030081
C	-1.3968906	-0.6293512	-0.6507043
C	-2.6105079	-1.3045721	-0.7156596
C	-3.7123138	-0.7318827	-0.1082843
C	-3.6533572	0.48449058	0.55136932
C	-2.437647	1.15128587	0.59396854
H	-2.3636104	2.1042209	1.10024914
H	-4.5399781	0.89080316	1.02054315
F	-4.8986229	-1.3892537	-0.1558979
H	-2.7024614	-2.254851	-1.2249986
H	-0.5288821	-1.0672248	-1.1257798
N	-0.0625964	2.64593401	0.05551199
H	0.87528625	3.04588073	0.11130832
H	2.20146516	1.87660572	-1.4562128
H	4.38270689	0.69255991	-1.397208
F	4.90568693	-1.3441193	0.11746112
H	2.85231782	-2.0022946	1.55390558

$C_{26}H_{16}F_4N_2$

C	-5.3019437	-0.3791872	0.3919993
C	-5.4812199	-1.3571919	-0.5677894
C	-4.4647874	-1.7628601	-1.4170687
C	-3.220549	-1.1640629	-1.2898682
C	-2.9921475	-0.1652255	-0.3320653
C	-4.0511486	0.21801026	0.5000739
H	-3.8993023	0.98043871	1.25251419
C	-1.6478547	0.4473298	-0.191716
C	-1.5384826	1.84219954	0.31709849
C	-2.3114707	2.85610495	-0.2614294
C	-2.2044801	4.17301165	0.16821713
C	-1.3309593	4.45551714	1.20280083
C	-0.5608991	3.48299317	1.81446133
C	-0.6641408	2.17489167	1.35754338
H	-0.0677928	1.40643614	1.82950655
H	0.10351111	3.746942	2.62683496
F	-1.2286718	5.73743023	1.63794199
H	-2.7871188	4.96481553	-0.2841192
H	-2.9958309	2.61971226	-1.0663887
N	-0.6420984	-0.2900374	-0.5301465

N	0.59336925	0.31224338	-0.5730293
C	1.62375534	-0.4358701	-0.3529692
C	1.55714585	-1.8494701	0.10948955
C	2.27393782	-2.8391806	-0.5738402
C	2.20285992	-4.17182	-0.1874547
C	1.42379743	-4.4952342	0.9087495
C	0.71278618	-3.5482022	1.62319907
C	0.77770219	-2.2232968	1.20963767
H	0.22693547	-1.4744937	1.76178017
H	0.12238351	-3.8442493	2.4804243
F	1.35796539	-5.7932707	1.30158574
H	2.74162387	-4.9447458	-0.7197542
H	2.88481325	-2.5709111	-1.426513
C	2.95152379	0.18387672	-0.5873648
C	4.07902164	-0.2294531	0.13288664
C	5.31647499	0.37354988	-0.0617435
C	5.41228213	1.3882161	-0.9950857
C	4.32572958	1.82469843	-1.7352586
C	3.09647715	1.21936244	-1.5222343
H	2.23404941	1.54293059	-2.088869
H	4.44812839	2.61629964	-2.4631208
F	6.61800942	1.97795413	-1.1983499
H	6.18921882	0.06587491	0.49920512
H	3.99268403	-1.0206265	0.86576267
H	-2.4118897	-1.4639882	-1.942298
H	-4.6521363	-2.52596	-2.1613648
F	-6.7011699	-1.9407576	-0.6867737
H	-6.1213935	-0.094936	1.03907689

9. Assessment of Overpotential with a Ruthenium Polypyridyl Complex

The approach to the thermodynamics of N_2/NH_3 in THF is adapted from Miller et al. for the interconversion of N_2, NH_3, N_2H_4 and N_2H_2 in acetonitrile.[7] The method employs buffered electrolytes to ensure a stable thermodynamic reference point, and the H^+/H_2 open-circuit potential (OCP)[8] was measured under the non-aqueous reaction conditions to enable conversion of aqueous to non-aqueous thermodynamic data. It has been reported that the saturated concentration of ammonia in THF is 0.34 M,[9] and the $\Delta G°$ of $NH_3(g)/NH_3(THF)$ is calculated to be 0.64 kcal/mol (Scheme S5, eq i). The H^+/H_2 open-circuit potential (OCP) was measured to be -0.86 V vs Fc^+/Fc under conditions of NH_4PF_6 (0.2 M, 326 mg), saturated ammonia in THF (10 mL) and 1 atm of hydrogen atmosphere (via bubbling hydrogen gas into the solution). The arithmetic yields the thermodynamic potential of ammonia oxidation to dinitrogen, which is -0.81 V vs Fc^+/Fc.

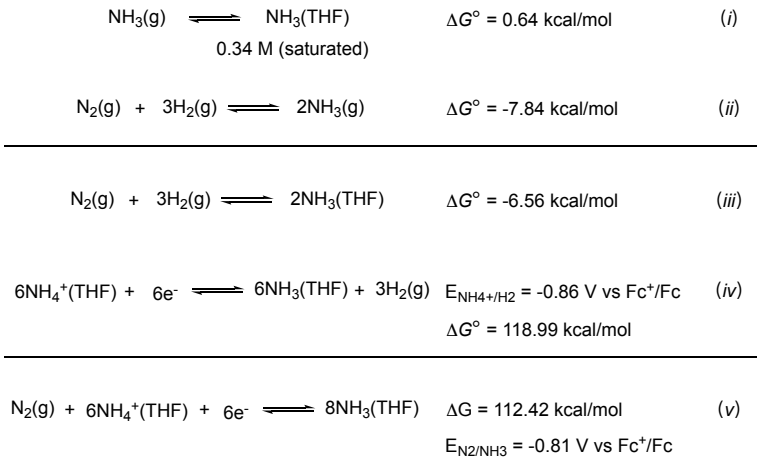

Scheme S5. Thermodynamic determination of N_2/NH_3 couple in THF.

10. Compounds Characterization

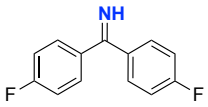

This compound is synthesized following a reported procedure for benzophenoneimine synthesis.[10] In a 3-neck flask, 150 ml of dry toluene was chilled in an ice-bath under nitrogen. A portion of 4,4'-difluorobenzophenone (20 mmol, 4.36 g) was added and allowed to dissolve. At this point, 22 ml of $TiCl_4$ (1.0 M in toluene) was added slowly, leading to a yellow precipitate. The nitrogen purge of the flask was halted, and gaseous NH_3 was introduced to the solution by a gas dispersion tube until saturation. The suspension became green and stirred overnight. Then, 250 ml of saturated aqueous sodium carbonate was added and stirred for 10 min. The layers were separated, and the organic layer was extracted with 75 ml saturated sodium carbonate and then 75 ml of brine. The first aqueous phase was extracted with two 100 ml portions of ethyl acetate, which were in turn extracted with 75 ml of brine. The combined organic solutions were dried over sodium sulfate, filtered and concentrated by rotary evaporation to give the titled product as light yellow oil (3.57 g, 82% yield). The product is used without purification. The spectral data are available in the literature.[11]

^{1}H NMR (400 MHz, $CDCl_3$) δ 9.67 (s, 1H), 7.55 (s, 4H), 7.09 (t, J = 8.6 Hz, 4H). ^{13}C NMR (100 MHz, $CDCl_3$) δ 175.8, 163.9 (d, J = 250.7 Hz), 135.2, 130.3, 115.3 (d, J = 21.7 Hz). ^{19}F NMR (377 MHz, $CDCl_3$) δ -109.83 (s).

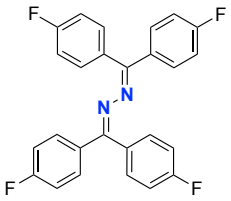

After bulk electrolysis of iodide-mediated system, the reaction solution was concentrated by rotary evaporation. The residue was purified via column chromatography on silica gel with hexane/ethyl acetate (5:1) as eluent to give the azine as yellow solid (87.6 mg, 81% isolated yield).

^{1}H NMR (400 MHz, $CDCl_3$) δ 7.53 – 7.42 (m, 4H), 7.37 – 7.29 (m, 4H), 7.13 (t, *J* = 8.7 Hz, 4H), 7.00 (t, *J* = 8.7 Hz, 4H). ^{13}C NMR (100 MHz, $CDCl_3$) δ 163.9 (d, *J* = 250.9 Hz), 162.8 (d, *J* = 249.4 Hz), 158.8, 134.0 (d, *J* = 3.1 Hz), 131.4 (d, *J* = 8.2 Hz), 131.1 (d, *J* = 3.5 Hz), 130.6 (d, *J* = 8.5 Hz), 115.2 (d, *J* = 21.7 Hz), 115.1 (d, *J* = 21.6 Hz). ^{19}F NMR (377 MHz, $CDCl_3$) δ -110.44 (s), -111.22 (s).

HRMS (**ESI**) Calculated for $[M+H]^+$: 433.1322, measured: 433.1318.

11. NMR Spectra

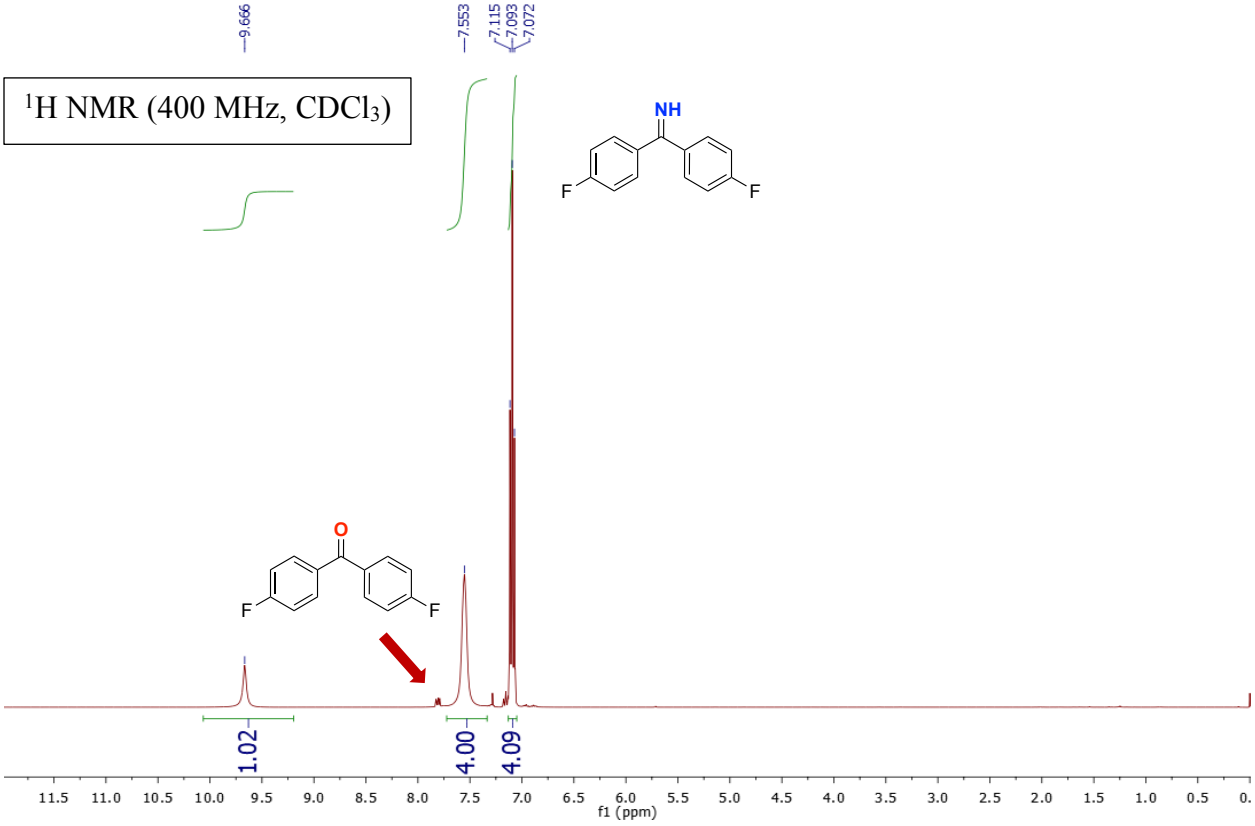

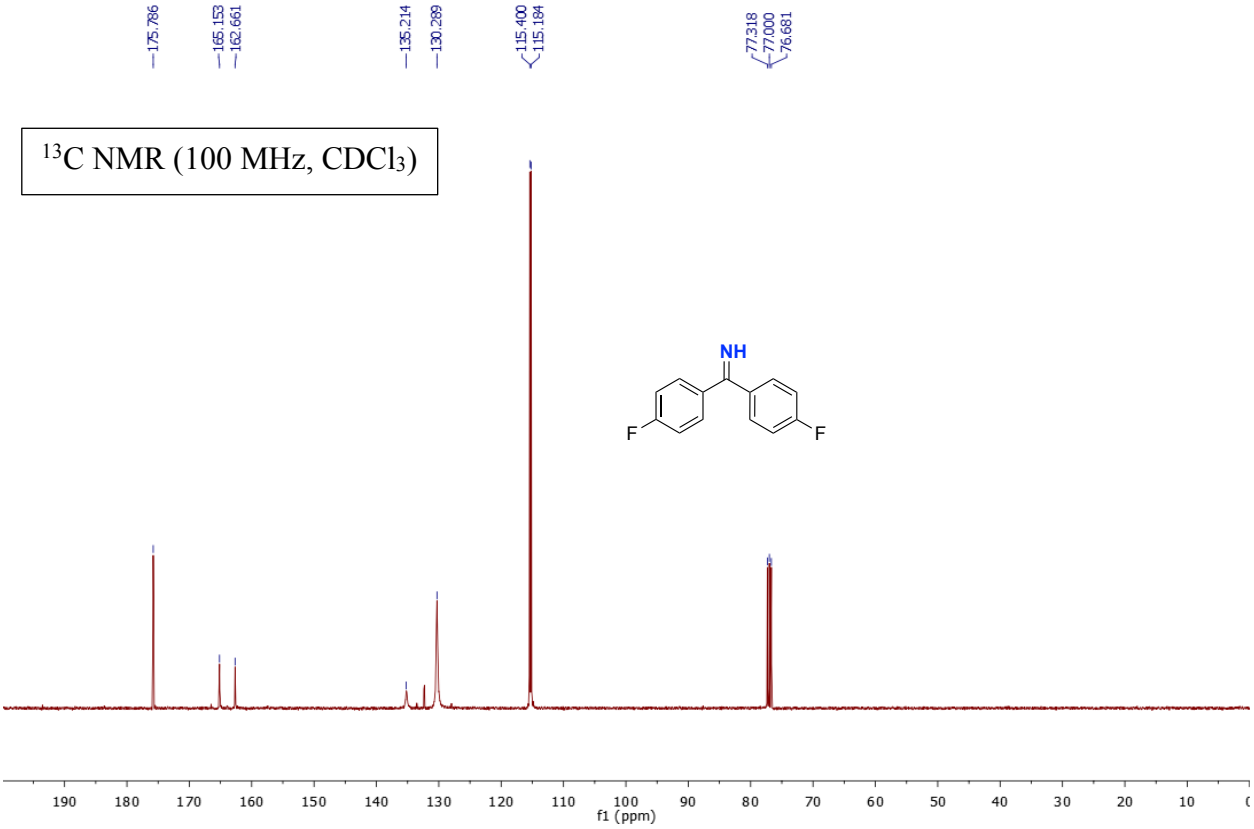

^{19}F NMR (377 MHz, $CDCl_3$)

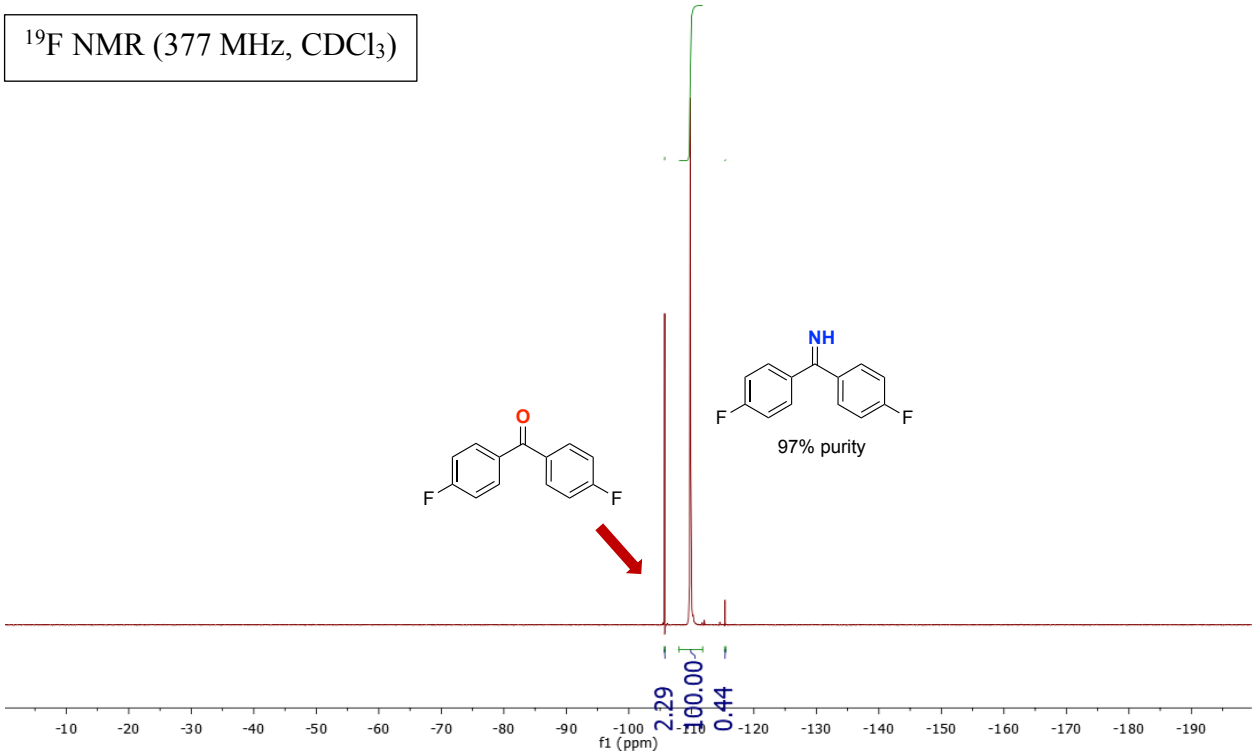

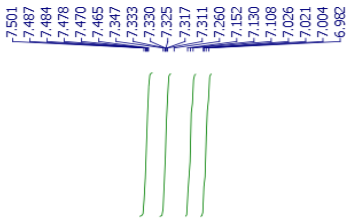

^{1}H NMR (400 MHz, $CDCl_3$)

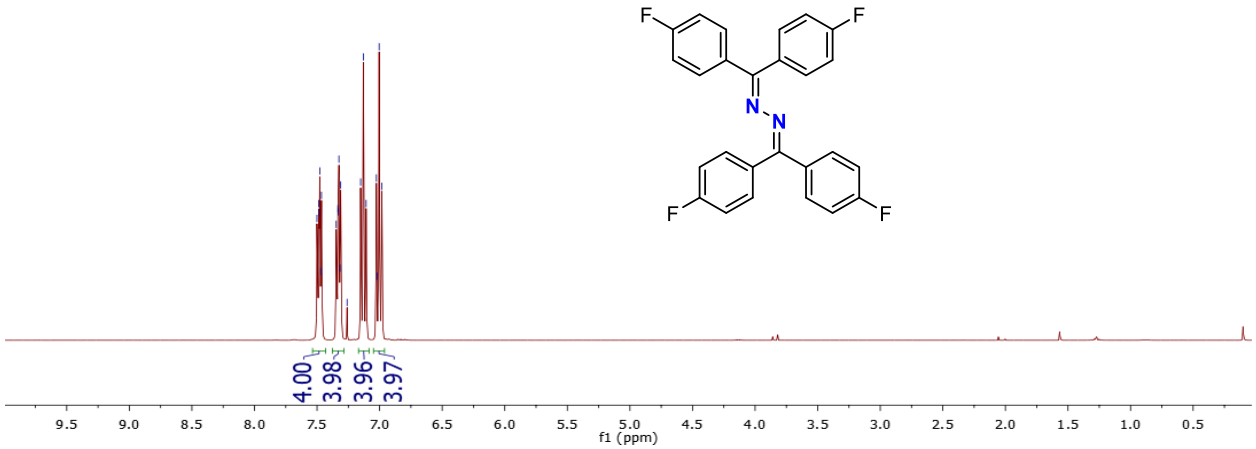

^{13}C NMR (100 MHz, $CDCl_3$)

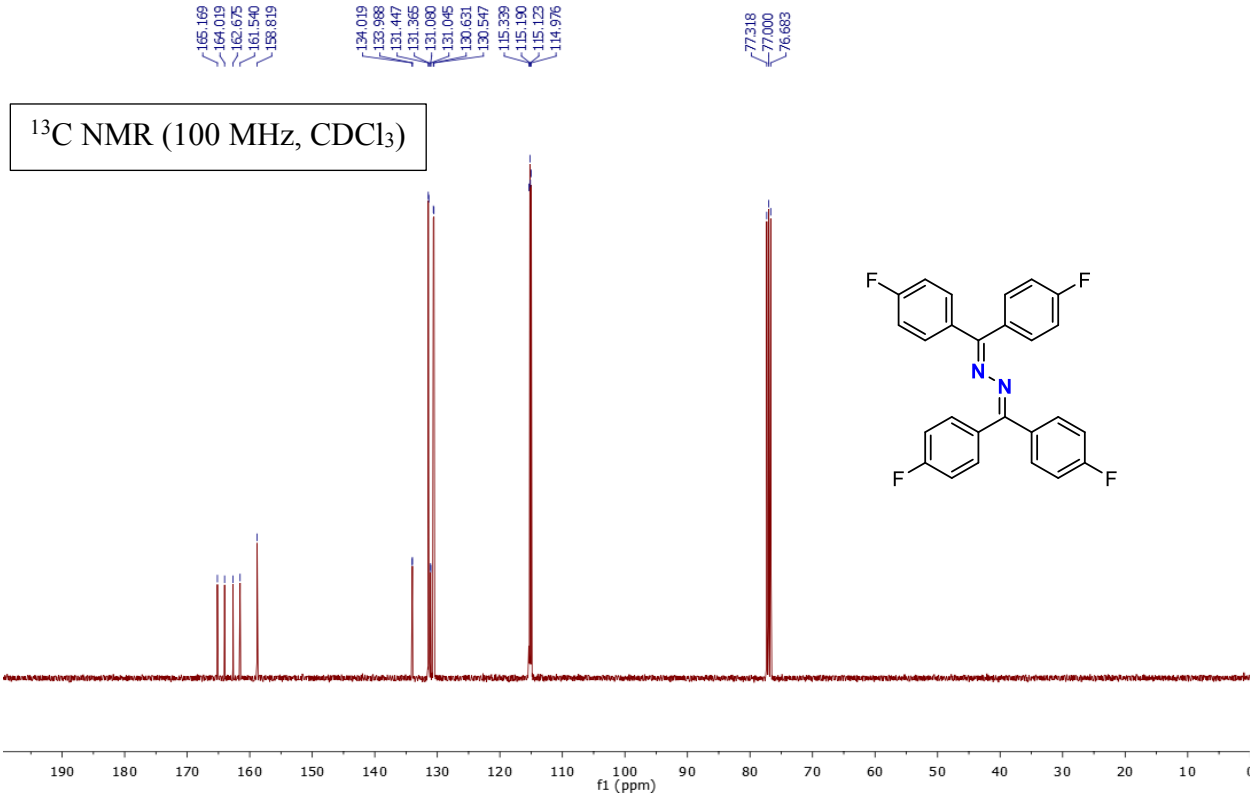

^{19}F NMR (377 MHz, $CDCl_3$)

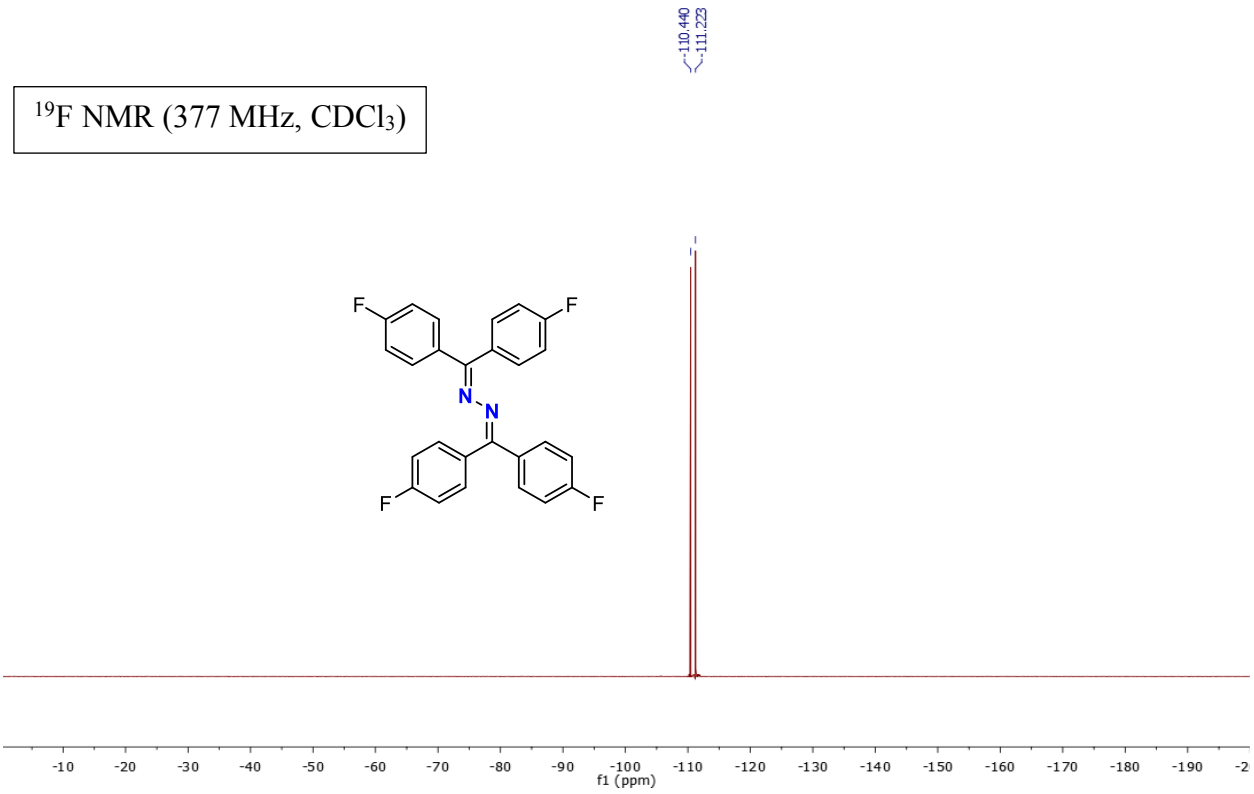

12. References

1. Nervi, C. http://lem.ch.unito.it/chemistry/esp_manual.html (accessed 6/3/2020).
2. Lindley, B. M.; Appel, A. M.; Krogh-Jespersen, K.; Mayer, J. M.; Miller, A. J. M. Evaluating the thermodynamics of electrocatalytic N_2 reduction in acetonitrile. *ACS Energy Lett.* **2016**, *1*, 698-704.
3. Choi, P. J.; Petterson, K. A. Roberts, J. D. Ionization equilibria of dicarboxylic acids in dimethyl sulfoxide as studied by NMR. *J. Phys. Org. Chem.* **2002**, *15*, 278-286.
4. Kaljurand, I.; Kütt, A.; Sooväli, L.; Rodima, T.; Mäemets, V.; Leito, I.; Koppel, I. A. Extension of the self-consistent spectrophotometric basicity scale in acetonitrile to a full span of 28 pK_a units: unification of different basicity scales. *J. Org. Chem.* **2005**, *70*, 1019-1028.
5. Eckert, F.; Leito, I.; Kaljurand, I.; Kütt, A.; Klamt, A.; Diedenhofen, M. Prediction of Acidity in Acetonitrile Solution with COSMO-RS. *J. Comput. Chem.* **2009**, *30*, 799-810.
6. *Gaussian 16* (Revision B.01), Frisch, M. J.; Trucks, G. W.; Schlegel, H. B.; Scuseria, G. E.; Robb, M. A.; Cheeseman, J. R.; Scalmani, G.; Barone, V.; Petersson, G. A.; Nakatsuji, H.; Li, X.; Caricato, M.; Marenich, A. V.; Bloino, J.; Janesko, B. G.; Gomperts, R.; Mennucci, B.; Hratchian, H. P.; Ortiz, J. V.; Izmaylov, A. F.; Sonnenberg, J. L.; Williams-Young, D.; Ding, F.; Lipparini, F.; Egidi, F.; Goings, J.; Peng, B.; Petrone, A.; Henderson, T.; Ranasinghe, D.; Zakrzewski, V. G.; Gao, J.; Rega, N.; Zheng, G.; Liang, W.; Hada, M.; Ehara, M.; Toyota, K.; Fukuda, R.; Hasegawa, J.; Ishida, M.; Nakajima, T.; Honda, Y.; Kitao, O.; Nakai, H.; Vreven, T.; Throssell, K.; Montgomery, Jr., J. A.; Peralta, J. E.; Ogliaro, F.; Bearpark, M. J.; Heyd, J. J.; Brothers, E. N.; Kudin, K. N.; Staroverov, V. N.; Keith, T. A.; Kobayashi, R.; Normand, J.; Raghavachari, K.; Rendell, A. P.; Burant, J. C.; Iyengar, S. S.; Tomasi, J.; Cossi, M.; Millam, J. M.; Klene, M.; Adamo, C.; Cammi, R.; Ochterski, J. W.; Martin, R. L.; Morokuma, K.; Farkas, O.; Foresman, J. B.; Fox, D. J. Gaussian, Inc., Wallingford CT, 2016.
7. Lindley, B. M.; Appel, A. M.; Krogh-Jespersen, K.; Mayer, J. M.; Miller, A. J. M. Evaluating the thermodynamics of electrocatalytic N_2 reduction in acetonitrile. *ACS Energy Lett.* **2016**, *1*, 698-704.
8. Roberts, J. A. S.; Bullock, R. M. Direct determination of equilibrium potentials for hydrogen oxidation/production by open circuit potential measurements in acetonitrile. *Inorg. Chem.* **2013**, *52*, 3823-3835.
9. Habibzadeh, F.; Miller, S. L.; Hamann, T. W.; Smith, III M. R. Homogeneous electrocatalytic oxidation of ammonia to N_2 under mild conditions. *Proc. Natl. Acad. Sci. U.S.A.* **2019**, *119*, 2849-2853.
10. Brenner, D. G.; Cavolowsky, K. M.; Shepard, K. L. Imino-bridged heterocycles. IV [1]. A facile synthesis of sulfenimines derived from diaryl ketones. *J. Heterocyclic Chem.* **1985**, *22*, 805-808.
11. He, R.; Huang, Z.-T.; Zheng, Q.-Y.; Wang, C. Manganese-catalyzed dehydrogenative [4+2] annulation of N–H imines and alkynes by C–H/N–H activation. *Angew. Chem. Int. Ed.* **2014**, *53*, 4950-4953.